Theor. Comput. Fluid Dyn. (2009) 23: 15–36
DOI 10.1007/s00162-009-0093-x

ORIGINAL ARTICLE

Paul Manneville · Olivier Czarny

Aspect-ratio dependence of transient Taylor vortices close to threshold

Received: 20 November 2007 / Accepted: 27 January 2009 / Published online: 20 February 2009

Abstract We perform a detailed numerical study of transient Taylor vortices arising from the instability of cylindrical Couette flow with the exterior cylinder at rest for radius ratio $\eta = 0.5$ and variable aspect ratio Γ. The result of Abshagen et al. (J Fluid Mech 476:335–343, 2003) that onset transients apparently evolve on a much smaller time–scale than decay transients is recovered. It is shown to be an artefact of time scale estimations based on the Stuart–Landau amplitude equation which assumes frozen space dependence while full space–time dependence embedded in the Ginzburg–Landau formalism needs to be taken into account to understand transients already at moderate aspect ratio. Sub-critical pattern induction is shown to explain the apparently anomalous behaviour of the system at onset while decay follows the Stuart–Landau prediction more closely. The dependence of time scales on boundary effects is studied for a wide range of aspect ratios, including non-integer ones, showing general agreement with the Ginzburg–Landau picture able to account for solutions modulated by Ekman pumping at the disks bounding the cylinders.

Keywords Taylor–Couette instability · Transient dynamics · Numerical approach

PACS 47.20K, 47.54B, 47.11K

1 Introduction

Taylor–Couette (TC) instability, the instability of a flow between two coaxial cylinders in differential rotation, is a good example of super-critical cellular instability,[1] i.e. a stationary instability at finite critical wave-vector gently saturating beyond threshold [5–7]. As such, it has been the subject of so many studies [8] that one might think that everything had been said about it or, at least, that *dynamical systems theory* should give us technical tools to overcome problems that might appear at a quantitative level without need of qualitatively new concepts. Observations made by Abshagen et al. [1] precisely take place in this context. They studied the *transient* regime toward steady TC vortices in the vicinity of the instability threshold R_c, where R, the Reynolds number to be defined later, is the control parameter. Series of laboratory and computer experiments were performed

[1] To be more precise, this is the case when the two cylinders rotate in the same direction or the inner cylinder is at rest, since when they rotate in opposite directions, the bifurcation may be sub-critical and the situation is more complex, especially when they are rotating fast, see e.g. [2–4].

Communicated by P. Hall

P. Manneville (✉)
Laboratoire d'Hydrodynamique, École Polytechnique, Palaiseau, France
E-mail: paul.manneville@ladhyx.polytechnique.fr

O. Czarny
M2P2, UMR 6181 CNRS, Universités d'Aix-Marseille, I.M.T. La Jetée, Technopôle de Château-Gombert,
13451 Marseilles Cedex 20, France

starting from equilibrium solutions at some given $R = R_i$ by imposing some final value $R = R_f$ impulsively at $t = 0$. They considered moderately large aspect ratios $\Gamma = \ell/d$, where ℓ is the length of the cylinders and d the gap between them, and explored the *decay* case corresponding to $R_f < R_i$ as well as the *onset* case with $R_f > R_i$. Their most striking result, obtained for $R_f > R_c$ and approaching R_c from above, was the observation of a discrepancy between characteristic time scales at onset and decay, onset times being much shorter than decay times, at variance with what is expected from the universal behaviour accounted for by the classical Landau formulation at a super-critical bifurcation. Furthermore, the discrepancy was dramatically amplified as Γ was increased. Whether or not these results can be understood within a known framework is the subject of the present paper. To be more precise, we shall show that the time constant estimates based on apparently good fits to solutions to the plain Stuart–Landau equation without forcing, Eq. 2 below, as obtained in [1], display systematic deviations that make them misleading, that taking into account end forcing in a naive way, Eq. 4, improves the state of affairs just a little but remains insufficient, and that fully unfreezing the space dependence is necessary. This will be done at a semi-quantitative level using the Ginzburg–Landau envelope equation, Eq. 6, and the phase diffusion equation, Eq. 8, as means to rationalise our observations based on numerical simulations of the Navier–Stokes equations.

In Sect. 2, we come back to the specificity of lateral boundary effects in the TC experiment and discuss the setting in more detail. Subsequent sections are devoted to a presentation of results from our computer experiments. A brief account of the numerical implementation and associated post-treatment tools is given in Sect. 3. We next turn to a presentation of transient experiments in conditions approaching those of [1]. Onset ($R_i < R_f$) and decay ($R_i > R_f$) experiments are analysed for a set of values of R_f approaching R_c in Sect. 4, but a single (already large but not so large) value $\Gamma = 24$ is examined. The rest of the paper is devoted to the interpretation of the observed discrepancy from our simulation results for Γ in the range 8–40. We study the different stages of the transients depending on the type of experiment, onset or decay, and the value of Γ, in order to extract quantitative trends associated to these stages. We also examine decay towards sub-critical states ($R_f < R_c$) in Sect. 6 and onset at aspect ratios that do not fit an integer number of pairs of rolls in Sect. 7. The first case was partially considered by Abshagen et al. (their Figs. 2 and 4) and the second one not at all. Section 8 gathers our conclusions.

2 Bifurcation theory and lateral boundary effects

Schematically, in the limit of infinite aspect ratio, a uniform TC pattern close to onset is searched in the form

$$V = A(t)\exp(iq_c z) + cc\,, \tag{1}$$

where V represents any physically relevant field, A is a complex scalar amplitude and q_c the critical wave-vector accounting for the space dependence at threshold along the direction of periodicity here called z; cc denotes complex conjugation. Any other spatial dependence, irrelevant here, is dropped. At lowest non-trivial order, the temporal dependence of such a uniform pattern is all contained in that of A governed by a *Stuart–Landau equation* [9]:

$$\tau_0 \tfrac{\mathrm{d}}{\mathrm{d}t} A = \varepsilon A - g|A|^2 A\,, \tag{2}$$

where $\varepsilon = (R - R_c)/R_c$ is the reduced control parameter, τ_0 a characteristic time, and $g = 1/A_0^2$ the coupling constant accounting for non-linear saturation effects beyond threshold, A_0 being the natural amplitude scale ($g > 0$ for a super-critical bifurcation). Equation (2) is the normal form for a super-critical pitchfork bifurcation in the presence of translational invariance, which is reflected by the fact that the phase of the complex amplitude A is not fixed by the equation and can be eliminated through a change of the origin of the z coordinate. It is also called a *circle pitchfork* bifurcation. Once the phase is fixed, one gets two solutions, π-shifted from one another, with $|A| = A_0\sqrt{\varepsilon}$. This shift corresponds to a translation by $\lambda_c/2$ where $\lambda_c = 2\pi/q_c$ is the critical wavelength. Ideal steady states as obtained from (2) were derived by e.g. Stuart [10], Kirchgässner [11], or Davey [12].

Upon time rescaling, the Landau equation provides a universal framework to interpret the onset/decay of Taylor vortices after impulsive change of the rotation rate of the inner cylinder, see the very early work of Donnelly and Schwarz [13]. Results reported by Abshagen et al. [1] relate to that kind of analysis for realistic finite geometry covering a wide range of variable but moderate aspect ratios, with the conclusions alluded to previously contradicting the universality assertion. The absolute value of the radial velocity at mid-gap and

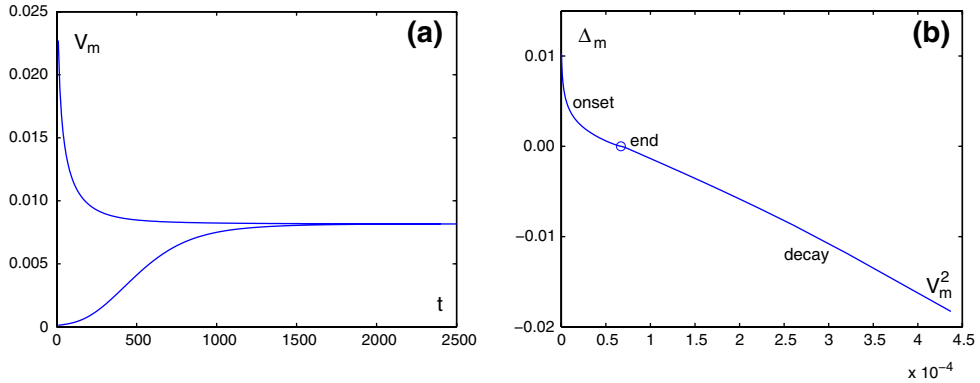

Fig. 1 **a** Time series of V_m during *onset* from $R_i = 67.2$ to $R_f = 68.7$ (*lower curve*) and *decay* from $R_i = 74.5$ to $R_f = 68.7$ for $\Gamma = 24$ (*upper curve*). **b** Test of the Landau assumption: behaviour of $\Delta_m = \frac{\mathrm{d}}{\mathrm{d}t} \ln V_m$ as a function of V_m^2 during the same onset/decay experiments; final steady state value marked with an open circle; onset (*decay*): part of the curve to the left (*right*) of the open circle, with $\Delta_m > 0$ ($\Delta_m < 0$). The critical Reynolds number for $\Gamma \to \infty$ is $R_c \approx 68.186$ [14]

mid-length of the cylinders, denoted V_m later on, was used as a proxy to the amplitude $|A|$. The observed unexpected behaviour of the time scales near threshold was detected by fitting $V_m(t)$ against the solutions to (2). Decay and onset characteristic times were found equal (as expected) only in numerical simulations when fictitious stress-free conditions at the end disks were adopted. On the contrary, a marked dependence of the characteristic times on the type of experiment, onset or decay, and the aspect ratio Γ was observed with realistic no-slip conditions.

An immediate empirical indication that the strict Landau scheme is not a good basis to analyse the data can be obtained by rewriting (2) as $\tau_0 |A|^{-2} \frac{\mathrm{d}}{\mathrm{d}t} |A|^2 = 2(\varepsilon - g|A|^2)$ or after slight simplification:

$$\tau_0 \frac{\mathrm{d}}{\mathrm{d}t} \ln(|A|) = \varepsilon - g|A|^2 \,. \tag{3}$$

If V_m were a good proxy to the amplitude $|A|$, then its logarithmic derivative, $\Delta_m = \frac{\mathrm{d}}{\mathrm{d}t} \ln V_m$, would behave linearly with V_m^2. Our results for $\Gamma = 24$ are displayed in Fig. 1 which shows that this is markedly not the case for onset, while agreement seems more reasonable for decay. A paradox is that onset seems slower than decay in Fig. 1a. In contrast, if the framework underlying (3) is valid, the evolution rates are given by the local slopes of the curves in its panel (b) and obviously the decay rate is smaller than any local onset rate (except near the end) or any (or average) onset rate. Stated otherwise, according to these estimates, the decay time remains larger than the onset time though this contradicts the visual impression of a fast exponential decay toward some new saturated state (upper curve). Onset appears slower because it is made of exponential growth from a low amplitude state followed by exponential relaxation toward the same saturated state (lower curve).

The logical consequence is that the Stuart–Landau equation, undoubtedly valid for ideal patterns in the infinite aspect-ratio limit, fails due to the presence of lateral boundaries at finite distance. Their qualitative effect is to break translational invariance but, if the lateral boundaries are far enough, the so-introduced perturbation should be small. This can tentatively be modelled by adding a constant quantity[2] H to the right-hand-side of (2) which then reads:

$$\tau_0 \frac{\mathrm{d}}{\mathrm{d}t} A = \varepsilon A - g|A|^2 A + H \,. \tag{4}$$

Phase invariance of (2) is broken and the bifurcation at $R = R_c$ (i.e. $\varepsilon = 0$) is destroyed. As a result, out of the double family of possible steady-state solutions to (2) with arbitrary phases shifted by π in the *perfect* bifurcation case, in the *imperfect* case a single solution is selected with well defined phase, forming a branch of states continuously connected to the base state as ε is varied from negative to positive values. Another

[2] In a thermodynamic context, the Landau theory of phase transitions with an order parameter would introduce H as the magnetic field conjugate to the magnetisation M, the order parameter of the paramagnetic-ferromagnetic transition and (4) would describe the relaxation of M in the presence of H as $\tau_0 \frac{\mathrm{d}}{\mathrm{d}t} M = -\partial \mathcal{F}/\partial M$, where $\mathcal{F}(M, H) = -\frac{1}{2}\varepsilon M^2 + \frac{1}{4} g M^4 - MH$ would be the thermodynamic free energy of the system, and $\varepsilon = (T_c - T)/T_c$, T_c being the critical temperature below which the system is magnetically ordered in the absence of H.

branch of steady states, formed with the remnants of the formerly unstable base state and π-shifted solution, appears through a saddle-node bifurcation somewhat beyond R_c ($\varepsilon_{sn} > 0$). The introduction of the constant H in (4) is purely phenomenological. More technical answers to the bifurcation problem in the presence of lateral boundaries specific to the TC flow were given e.g. by Schaeffer [15] or Hall [16] for small aspect-ratio systems. When the aspect-ratio increases, the infinite domain limit becomes a more relevant starting point and boundary effects are better studied in terms of modulations (envelope) to the ideal state of vortices with uniform strength (amplitude).

For Rayleigh–Bénard convection, it is not too difficult to achieve experimental conditions under which the fluid layer heated from below stays strictly at rest by carefully controlling the horizontality of the set-up and the thermal conductivity of the lateral walls. Accordingly, the expected perfect bifurcation is actually obtained or else the imperfection can remain small and under control. In contrast, the purely azimuthal base flow below threshold assumed by the analytical theory of the TC instability cannot be realised in a typical experimental set-up: the gap between the cylinders is usually closed at their ends by disks that are fixed to one of the cylinders, inner or outer, and the no-slip boundary condition posed on the velocity field at the disks implies the presence of a recirculation which modifies the base Couette profile.

The physical perturbation brought to the mathematical bifurcation problem has special features since it is always *large* but stays localised in a narrow region close to the disks so that its effect on the system as a whole may seem to remain *small*. The effectiveness of the perturbation stems from the fact that it does not decrease as the threshold is approached as would be the case if its amplitude were scaling as a strictly positive power of ε, but on the contrary remains finite independently of the mechanism generating the Taylor vortices, i.e. it is $\mathcal{O}(\varepsilon^0)$. Except when considering numerical experiments with artificial end conditions [15] the global perturbation so introduced is beyond control and turns out not to be small, even in an extended geometry when the aspect ratio Γ is large: the presence of lateral boundaries does have stronger non-trivial consequences than for convection. In the TC case, the remnants of the π-shifted solutions appear only far above threshold, forming what are known as *anomalous* states discovered by Benjamin and studied long ago [17]. Remarkably, the branch of anomalous states ends at a turning point that does not approach the critical point of the perfect bifurcation ($\varepsilon = 0$, $A = 0$) as the perturbation is artificially decreased, while the branch of *regular* modes, connected to the basic state, behaves as expected at an usual imperfect bifurcation point with decreasing imperfection. An analysis of the mathematics of the full bifurcation diagram has been performed by Rucklidge and Champneys on a model system [18], clarifying the distinction between *regular* and *anomalous* states.

In their work Abshagen et al. only considered transients toward regular states. As can already be understood from their Fig. 4 and will be illustrated further in Sects. 5 and 6, decay and onset transients are in fact profoundly different in character, which is not reflected in the plain Landau approach. On the one hand, the decay transient seems to display a single stage of on-the-spot collapse of the amplitude at a rate close to that predicted by the naive amplitude theory. On the other hand, at onset, for large enough systems ($\Gamma \gg 1$) one first observes the propagation of fronts coming from both ends and meeting at mid-length of the system and next the amplitude gets approximately uniform [19].[3] This mere observation gives us an immediate clue to systematic deviations from the Stuart–Landau prediction for onset contrasting with mild departure for decay: at lowest order, the cubic term in (2) directly derives from the self-interaction of a non-linear mode that basically keeps the analytical shape of the critical mode, which is nearly the case for early decay, but not at onset and moderate to large Γ, making (2) and its corrected version (4) both inappropriate, only slightly for decay but quite severely for onset.

Except for very short systems, or for uniform solutions under strict periodic boundary conditions, the assumptions underlying the derivation of (2) indeed fail and the solutions are better analysed by including the possibility of amplitude and phase *modulations* around the ideal periodic solution with critical wave-vector q_c:

$$V = A(z,t)\exp(iq_c z) + cc, \quad A(z,t) = |A(z,t)|\exp(i\phi(z,t)). \tag{5}$$

This is certainly necessary here due to the local character of the perturbation triggering the Taylor vortices at each cylinder end for any finite Γ. These problems were much studied in the 1980's, in particular thanks to the explicit development of *envelope formalisms*. In the simple case of a super-critical cellular instability of interest here, when modulations depend on a single space coordinate z referring to a periodic solution with

[3] Onset transients have a long story, especially when front propagation became under focus in connection with wavelength selection beyond threshold in semi-infinite geometry, see e.g. [20,21] and references therein.

wave-vector q_c, one then arrives at a *Ginzburg–Landau equation* with real coefficients, consistent at order $\varepsilon^{3/2}$ [9]:

$$\tau_0 \partial_t A = \varepsilon A + \xi_0^2 \partial_{zz} A - g|A|^2 A\,, \tag{6}$$

where the additional parameter ξ_0, the coherence length, measures how easily the unstable mode can accommodate modulations.[4] The quantity $A(z, t)$ generalising the scalar amplitude $A(t)$ introduced in the Stuart–Landau equation (2) is thus now a field variable, see e.g. Chapter 8 of [23] for technical details. Envelope modulations associated to finite size effects are then accounted for by boundary conditions set on A. Such conditions have been derived for Rayleigh–Bénard convection which, as said earlier, usually corresponds to a mild case [24–26]. Within the same framework, things are more involved in the TC case. Graham and Domaradzki [27] showed that the $\mathcal{O}(\varepsilon^0)$ localised perturbation at the disks implies a divergence of the amplitude with the distance to the lateral boundary at z_b as $A \sim (z - z_b)^{-1}$. This result is easily recovered by balancing $\xi_0^2 \partial_{zz} A$ and $g|A|^2 A$ in (6) with the corresponding space dependence for A close to the boundary. Solving (6) in the real case under this constraint, they could obtain a good account of the equilibrium solutions at finite aspect ratio close to threshold, first analysed in that perspective by Pfister and Rehberg [28]. Steady states considered by Pfister & Rehberg and Graham & Domaradzki were obtained for real envelopes and not complex ones as implied in (6). No wavelength adjustment could be accounted for since local wave-vector corrections are, by assumption, contained in the space derivative of the phase ϕ of the complex envelope as defined in (5). This limitation was overcome by Zaleski [29] who studied (6) with A complex and general boundary conditions at z_b in the form $A(z_b) = A_b$, with complex $A_b \sim \mathcal{O}(1)$. Interestingly, the introduction of this somewhat artificial constant[5] led to a non-trivial wavelength adjustment in case of a mismatch between the length of the system and a multiple of the critical wavelength, at first numerically observed, and next analytically derived from (6). The adjustment produced a minimum of the amplitude's modulus in the middle of the system and an Eckhaus-like instability when the mismatch was too large. This observation will motivate the study presented in Sect. 7.

The main objective of the present work is thus to document the different stages and associated scalings of the transients quantitatively, in order to clarify their role in the differences between characteristic times for onset or decay measured at moderate aspect ratios as reported by Abshagen et al. [1]. We shall show that at given Γ (here $\Gamma = 24$), results for *decay* can be approximately but consistently interpreted using (4) which, in turn, cannot explain the outcome of the *onset* experiments. Then we shall examine the effects of shape and wavelength adjustments within the envelope formalism (6) and shall interpret the latest stages of the transients using the concept of phase diffusion [30]. Having at our disposal a reliable numerical implementation of the Navier–Stokes equation in Couette geometry [33], we have chosen to use it to get realistic but fully numerical results. In contrast with laboratory experiments that are blurred with noise rendering the results in the long-time limit somewhat imprecise, the simulations could be performed up until complete convergence with great accuracy. We shall interpret them as quantitatively as possible and compare them with previous findings whenever available, rather than develop a much lighter analysis of transients relying on the model used by Rucklidge and Champneys [18] made time-dependent, or even follow Zaleski's phenomenological approach [29].

3 Geometry, numerical implementation, and post-treatment

To stick to the conditions of experiments reported in [1], we consider an annular cavity delimited by two coaxial cylinders of inner and outer radii r_i^* and r_o^* (hereafter, $*$ indicates dimensional lengths). The inner cylinder rotates at Ω_i while the outer cylinder and the end-walls remain at rest (Fig. 2). The flow is governed by the three-dimensional incompressible Navier–Stokes equations in the usual velocity-pressure formulation and written in a cylindrical coordinate system (r^*, θ, z^*) with respect to an absolute frame of reference, see e.g. [5].

Dimensionless parameters specifying the geometry are the radius ratio $\eta = r_i^*/r_o^*$ and the aspect ratio $\Gamma = 2h^*/d^*$, where $2h^*$ is the length of the cylinders, and $d^* = r_o^* - r_i^*$ is the gap between them. The

[4] We consider axisymmetric TC vortices only. The mean-flow correction introduced by Hall [22] is therefore not relevant here (independently from the fact that it was derived in the small gap limit while we consider the case $\eta = 0.5$).

[5] For TC, this simple assumption is not compatible with the Ginzburg–Landau equation (6) which is consistent at order $\mathcal{O}(\varepsilon^{3/2})$ because, upon general rescaling, it says that the boundary effects scale like A, i.e. as $\mathcal{O}(\varepsilon^{1/2})$ and not as $\mathcal{O}(\varepsilon^0)$.

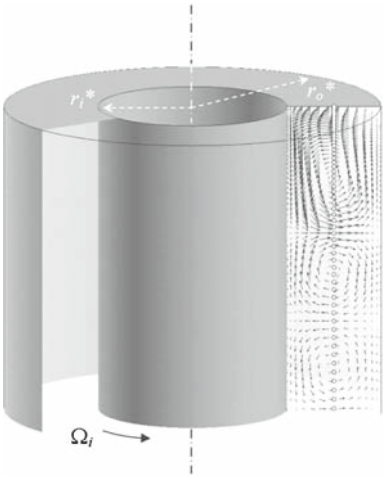

Fig. 2 Top of the Taylor–Couette system, $\eta = 0.5$. The inner cylinder rotates at Ω_i, the outer cylinder is fixed. One end-wall is represented on the top. On the right, velocity is projected on a meridian plane (r, z). The vertical line with white circles in this plane shows the points where v_r is recorded to obtain profiles as shown further in this paper

value $\eta = 0.5$ considered in [1] is kept here, while the range of Γ, 8–20, i.e. neither small nor extremely large, will be extended up to $\Gamma = 40$, in order to emphasise the trends. The Reynolds number is defined as $R = \Omega_i r_i^* d^*/\nu$, where ν is the kinematic viscosity of the fluid. For radius ratio $\eta = 0.5$, the critical Reynolds number is $R_c \approx 68.186$, see e.g. [14].

Equations are then written in dimensionless form using d^* and h^* to scale space along r^* and z^* respectively, $1/\Omega_i$ for time, and $\Omega_i r_i^*$ for velocity. The dimensionless axial and radial coordinates are $z = z^*/h^*$, so that $z \in [-1, 1]$, and $r = r^*/d^*$ or rather $y = (2r^* - r_o^* - r_i^*)/d^*$, so that $y \in [-1, 1]$. These particular rescalings fit the needs of the solver which uses Chebyshev polynomials along the two non-periodic directions.

The dimensionless velocity $\mathbf{v} = (v_r, v_\theta, v_z)$ obeys no slip boundary conditions at all rigid walls: $v_r = v_z = 0$, $v_\theta = 1$ at the inner wall ($y = -1$, $z \in [-1, 1]$), and $v_r = v_z = 0$, $v_\theta = 0$ at the outer wall ($y = +1$, $z \in [-1, 1]$). A singularity occurs at the junction between the stationary end-walls and the rotating inner cylinder ($y = -1$, $z = \pm 1$), which is handled by regularising the azimuthal velocity profile v_θ through an exponential interpolation in that corner:

$$v_r = v_z = 0\,, \quad v_\theta = \frac{\exp(-ay) - \exp(-a)}{\exp(a) - \exp(-a)} \quad \text{at} \quad z = \pm 1\,.$$

The width of the region where this exponential change occurs is set to $0.05d^*$ by adjusting the decay coefficient a. This small distance is consistent with gaps one typically finds between fixed end-walls and rotating cylinders in TC experimental set-ups. Regularisation effects are expected to be negligibly small away from the corners provided that this width is kept small enough. Here the regularisation function drops to zero over six collocation points next to the singularity,[6] which was found appropriate up to much higher Reynolds numbers with an equivalent numerical scheme in a slightly different configuration by Randriamampianina et al. [31]. With a different regularisation function and a different numerical approach in a similar case, Tavener et al. [32] used a comparable criterion so that we are confident that our quantitative results should not be sensitive to the presence of the singularity at the corner of the computational domain.

The 2D-axisymmetric solver is the same as that used in [33]. The method is based on a pseudo-spectral Chebyshev approximation which provides exponential convergence, see [34]. The set of flow variables $\Psi = (v_r, v_\theta, v_z, p)$ is approximated by a truncated series defined as:

$$\Psi_N(y, z, t) = \sum_{n=0}^{N_r-1} \sum_{m=0}^{N_z-1} \Psi_{nm}(t) T_n(y) T_m(z)\,,$$

where $N = (N_r, N_z)$ is the refinement of the mesh grid. Along (y, z) we use Gauss–Lobatto points $(y_i, z_j) \in [-1, 1]^2$, where $y_i = \cos(i\pi/(N_r - 1))$, $z_j = \cos(j\pi/(N_z - 1))$, with $0 \le i \le N_r - 1$ and $0 \le j \le N_z - 1$.

[6] Physically, this represents 2.5% of the gap while the Ekman-induced end vortex is about 1.3 gap width.

They correspond to the extrema of the Chebyshev polynomials T_n and T_m defined as $T_k(x) = \cos(k \arccos(x))$, $x \in [-1, 1]$. The discretized Navier–Stokes equations are exactly satisfied at the Gauss–Lobatto points. We set $N_r = 31$ and N_z depending on the aspect ratio Γ as:

Γ	8	12	16	24	32	40
N_z	151	181	201	251	301	351

The time scheme is semi-implicit and second-order accurate. It is a combination of a second-order backward implicit Euler scheme for the temporal term, an explicit Adams–Bashforth scheme for the non-linear terms, and an implicit formula for the viscous diffusion term. The method uses a projection-correction algorithm to handle the velocity-pressure coupling, as explained in [35].

Notice that the scaling of z defined above is internal to the numerical scheme and that the solution profiles are everywhere presented with the axial coordinate made dimensionless using d^* hence, avoiding the introduction of a new notation, with $z \in [-\Gamma/2, \Gamma/2]$.

Though the full solution was available, as in previous studies we worked with the radial velocity profile at mid gap, $v_r(y = 0, z, t) \equiv V(z, t)$. A proxy to the envelope $A(z, t)$ was next extracted from this profile *via* a Hilbert transform. In signal processing, the Hilbert transform is a tool used to *demodulate* an approximately periodic 'signal' that is modulated in amplitude and/or phase [36]. The relevant approximate periodicity here lies in the dependence on the axial coordinate. Formally, the Hilbert transform is defined as

$$\hat{W}(z) = -\frac{1}{\pi}\,\mathcal{P}\int_{-\infty}^{\infty}\frac{W(z')}{(z - z')}\mathrm{d}z',$$

where $W(z)$ is the (real) signal under consideration, $\hat{W}(z)$ its transform, and $\mathcal{P}$ the Cauchy principal part of the integral. The transform constructs a signal which, when Fourier analysed, is phase-shifted by $-\pi/2$, component by component. The complex signal $Z(z) = W(z) + i\hat{W}(z)$ is called the corresponding *analytic signal*. Its Fourier transform $\tilde{Z}(q)$ is obtained by setting to zero all components of the Fourier transform of W with negative argument q, where q is the conjugate of z, and by doubling those with positive argument. The analytic signal $Z(z)$ itself is then recovered by computing the inverse transform of $\tilde{Z}$ (MATLAB macro `hilbert.m`). Extraction of the modulus $|Z|$, and phase φ then yield the envelope and local wavelength.

By a slight abuse of language, the modulus of the Hilbert transform of $V(z, t)$ will hereafter be called the *amplitude* of the solution. As will be seen, the so-obtained amplitude is not a properly demodulated representation of the solution, contrary to what one could have expected. The reason is that the solution has no special symmetry properties with respect to $y = 0$ as soon as the curvature parameter η is strictly smaller than 1 (i.e. $r^*_{i,o}$ not infinite). Amplitude $V(z, t)$ then lacks the symmetry $V(z + \lambda/2, t) = -V(z, t)$, where λ is the wavelength of the main periodic component, due to the presence of even harmonics, typically $a_1 \sin(2\pi z/\lambda) + a_2 \sin(4\pi z/\lambda)$. The way the Hilbert transform is concretely implemented, as explained above, yields here $a_1 \exp(2\pi i z/\lambda) + a_2 \exp(4\pi i z/\lambda)$ hence a squared modulus $a_1^2 + a_2^2 + 2a_1a_2 \cos(2\pi z/\lambda)$ that displays a substantial periodic component to be traced back to the presence of the second harmonic generated by non-linearities clearly visible somewhat beyond threshold.

The absolute value of the velocity at the centre, $|V(z = 0, t)| = V_m(t)$, was used by Abshagen et al. as a tracer of the amplitude of the solution and its evolution was fitted against the solution to the Stuart–Landau equation to define the time constants characterising the transients. In contrast, we adopt here a more empirical point of view and compute its instantaneous evolution rate without any assumption on the validity of the Landau approach since we have already shown its limitations. In addition to $V_m(t)$, we also monitor the width of individual Taylor vortices and/or the positions z_j of the zeroes of $V(z, t)$ as functions of time in order to point out the decoupling between space and time explicitly. Figure 3 illustrates the relation between the two but identical quantitative results are clearly expected from one or the other since the vortex boundaries are given by the zeroes of the z-derivative of V.

The instantaneous evolution rate of some quantity $b(t)$—this can be $V_m(t)$, the width w_j of a given Taylor vortex or the position z_j of a given zero of $V(z, t)$—is usually obtained from the logarithmic derivative of its variation in time, $\frac{\mathrm{d}}{\mathrm{d}t}\ln b = b^{-1}\frac{\mathrm{d}}{\mathrm{d}t}b$. When specifically considering the behaviour as $t \to \infty$ of a quantity b that relax to some finite value, $b(t) \to b_\infty \neq 0$, we will rather determine its *asymptotic* evolution rate from its time derivative $\frac{\mathrm{d}}{\mathrm{d}t}b$ in order to get rid of the value of b_∞ which has no interest in itself. Assuming that $b(t)$ converges

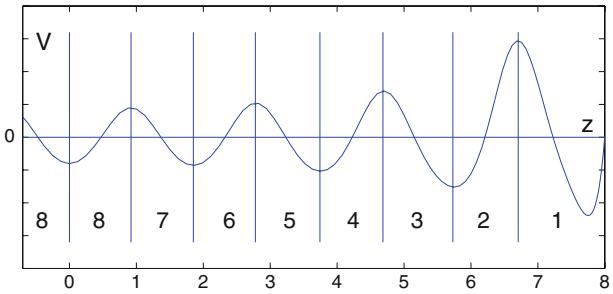

Fig. 3 Definition of Taylor vortices from $V(z,t)$, here illustrated using half of the onset solution at equilibrium for $\Gamma = 16$. Vortex boundaries correspond to local extrema of V, hence zeroes of $\partial_z V$ indicated by vertical lines. Vortex '1' appears to be larger since it has to include a boundary layer where the radial velocity drops to zero to meet the no-slip condition at the end disk (clamped to the external cylinder at rest in the laboratory frame), see also Fig. 2 displaying the velocity field; the symmetry of the solution is suggested by the replication of label '8'

exponentially fast toward b_∞, hence $b \approx b_\infty + \delta b \exp(-t/\tau)$, we shall get τ from $\ln\left(\left|\frac{\mathrm{d}}{\mathrm{d}t} b\right|\right) \sim -t/\tau$ up to a constant.

In order to get the best possible evaluation of the time constant governing the ultimate stage $t \to \infty$, we shall include the possibility of some curvature and fit the large-t tails of the curves against expressions in the form:

$$\ln(b(t)) = a_0 + a_1 t + a_2 t^2 \tag{7}$$

over the largest possible interval $[t_1, t_2]$, t_2 being taken as close as possible to the end of the simulation t_{end} (at the very end, differences were so small that what was registered was essentially numerical noise due to the limited number of digits kept in the records). The slope computed at t_{end} from (7) will give us the corresponding estimate in the limit $t \to \infty$. If, as we may expect, asymptotic relaxation is governed by a single global process, the set of values of τ corresponding to the different quantities b should collapse to a single value.

4 Experiments at $\Gamma = 24$

This experiment corresponds as closely as possible to that of Abshagen et al. in their Fig. 3, except that, for the moment, we consider a single value of the aspect ratio, namely $\Gamma = 24$, which is slightly larger than the largest value they considered.

• Let us first consider *decay* experiments. In addition to conditions corresponding to the preliminary test reported in Fig. 1 for $R_f = 68.7$, we studied the transients for $R_f = 68.5$, 68.3, 68.1, and 67.9, all starting from the equilibrium state at $R_i = 74.5$. The two values 68.1 and 67.9 are below the threshold for the infinite system $R_c = 68.186$ [14]. Using (3) to test the Landau assumption we obtain Fig. 4a which clearly shows that it holds reasonably well for all times and for all the values of R_f considered. Except near the end of the transient for sub-critical values, the relation between V_m^2 and Δ_m is indeed roughly linear and the downward shift from one curve to the next clearly corresponds to the change in ε. Fast on-the-spot collapse of the solution is particularly obvious from the inter-space between marks on the curves. If, at sub-critical R_f (67.9 and 68.1), the amplitudes were decaying exponentially to zero as for the infinite medium, the curves would intersect the vertical axis at negative values of Δ_m corresponding to the extrapolation of their leftmost part (see also Fig. 11 below for another illustration of the same phenomenon). On this basis, one can estimate the coefficients entering (2) using the five experiments (only the very first data points are used for $R = 67.9$ and 68.1). One then gets $g/\tau_0 \approx 46$ consistently and $\varepsilon/\tau_0 \approx 5.6 \times 10^{-3} R - 3.8 \times 10^{-1}$ which change its sign at $R = R_c^{\mathrm{ext}} \approx 68.15$, close to the infinite-system threshold value. From these estimates one gets $\tau_0 \approx 2.6$. Once differences between time-unit choices are correctly implemented, the above value compares favourably with the theoretical one given in [27]: $\tau_0 = 2.54$. The estimate of $A_0 = 1/\sqrt{g} \approx 0.09$ ($g \approx 120$)—also directly obtained from steady-states $V_m(t \to \infty) = A_0\sqrt{\varepsilon}$ with the estimated R_c for the three super-critical values of ε—can however not be directly related to the theoretical value since the comparison crucially involves the normalisation of the solution.

Let us now turn to the late stage of the transients and take (4) as a correction to (2). An estimate of the perturbation H would be obtained by setting $\varepsilon = 0$ in (4) and getting the corresponding value of $|A|^3$ by

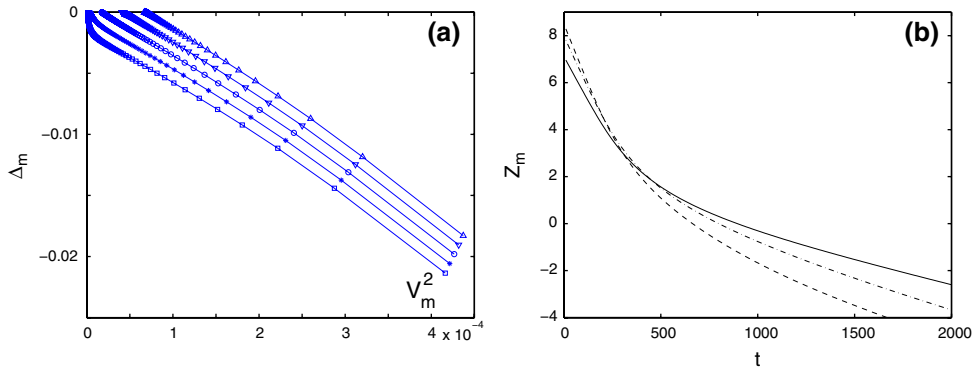

Fig. 4 **a** Test of the Landau assumption for decay (Up triangles: $R_f = 68.7$; down triangles: $R_f = 68.5$; open circles: $R_f = 68.3$; asterisks: $R_f = 68.1$; open squares: $R_f = 67.9$) one mark every $\delta t = 10$. **b** Quantity Z_m defined from the analytical solution to (2) should be a linearly decreasing function of time t if the equation were a valid approximation: here onset from $R_i = 67.2$ to $R_f = 68.3$ (solid line), 68.5 (dash-dotted), and 68.7 (dashed)

interpolation from the values for $R = 68.1$ and $R = 68.3$ bracketing the threshold. This leads to H ranging from 3.1×10^{-6} to 4.5×10^{-6} depending on whether one takes the extrapolated value $R_c^{\text{ext}} = 68.15$ or the theoretical one $R_c = 68.186$. In the same conditions solving (4) for $R = 67.9$ while assuming that it is sufficiently far from threshold to make $g|A|^3$ negligible (which can be checked afterwards), in the limit $t \to \infty$ one gets $|A| = H/r \approx 8.3 \times 10^{-4}$ or 1.1×10^{-3} to be compared to the measured value $V_m = 1.01 \times 10^{-3}$, which is not so bad in view of the approximations made all along the computation.

• We now examine whether the emerging picture is consistent with *onset* experiments. Starting from an initial state prepared at $R_i = 67.2$, we considered the values $R_f = 68.3$, 68.5, and 68.7. As anticipated from Fig. 1, the plain Landau test is strongly violated. This violation can be illustrated in a different way through a straightforward manipulation of the analytic expression of the solution to (2) which yields:

$$Z_m \equiv \ln(|(V_m^\infty / V_m(t))^2 - 1|) = -2t/\tau(\varepsilon)\,.$$

The characteristic time $\tau(\varepsilon)$ would then be obtained by fitting Z_m as a function of time against a straight line. Figure 4b displays the *systematic deviations* that forbid the evaluation of a single time scale $\tau(\varepsilon)$ in this way. This figure was obtained by suppressing the adjustable parameter V_m^∞ and replacing it by the value of V_m at the largest available time. When t approaches the end of the experiment, this approximation introduces a spurious logarithmic divergence which has not been displayed here since it is irrelevant to our purpose and does not change the main conclusion. In fact, the local slope of these curves can serve us to define instantaneous time scales $2/\tau(\varepsilon, t)$. Two regions are easily identified: the start which corresponds to the divergence from the initial condition, $V_m = V_m^0 \exp(t/\tau_{\text{start}})$, and the end which corresponds to the convergence from below towards the non-trivial solution, $V_m(t) = V_m^\infty - \delta V_m(t)$ with $\delta V_m \sim \exp(-t/\tau_{\text{end}})$. The argument behind the manipulation alluded to above shows that when the Stuart–Landau equation is valid $\tau_{\text{end}} = \tau_{\text{start}}/2$ and that the solution manages to keep $Z_m(t)$ varying linearly with t as $-2t/\tau(\varepsilon) + \text{Cst.}$ ($\tau = \tau_{\text{start}}$). This is obviously not the case here but τ_{start} and τ_{end} can still be defined from the data, either from the graph of Z_m or more directly from $\frac{\mathrm{d}}{\mathrm{d}t}\ln(V_m)|_{t=0}$ for τ_{start} and from $\ln(\frac{\mathrm{d}}{\mathrm{d}t}V_m)|_{t\to\infty}$ for τ_{end}, as explained at the end of Sect. 3. Results are gathered in the table below:

R	68.3	68.5	68.7
$1/\tau_{\text{start}}$	7.62×10^{-3}	8.98×10^{-3}	1.03×10^{-2}
$1/\tau_{\text{end}}$	1.94×10^{-3}	2.43×10^{-3}	2.64×10^{-3}
$H_{\text{start}}^{\text{estim}}$	2.07×10^{-6}	2.14×10^{-6}	2.21×10^{-6}
$H_{\text{end}}^{\text{estim}}$	9.42×10^{-7}	-8.66×10^{-6}	-2.58×10^{-5}

Remarkably, these rates both extrapolate to zero for $R \sim 67.2$, which is definitely below the threshold $R_c = 68.15$ (empirical, according to the first part of this study) or 68.19 (theoretical).

Obviously the perturbation introduced in (4) has to be taken into account. If this equation holds, for the initial part of the transient, neglecting the cubic term one gets $\tau_0 \frac{\mathrm{d}}{\mathrm{d}t}\ln(V_m(0)) = \varepsilon + H/V_m(0)$. Taking the

previous estimate for H, 3.1×10^{-6}, and using the value of V_m measured at $t = 0$, $V_m(0) = 1.2 \times 10^{-4}$ one obtains the value of R at which the growth rate is zero. This yields $R \sim 66.4$ in reasonable agreement with the extrapolated value mentioned above. Conversely, the formula can be used to compute new estimates for H as given in the third line of the table above. As expected they are consistently of the same order of magnitude as the previous one. The observed differences merely reflect the accumulation of uncertainties and approximations done all along the derivation (otherwise the observed and predicted values of R where the growth rate is zero would be in better agreement).

Considering $\tau_{\rm end}$, one observes that it is about a factor of four off $\tau_{\rm start}$. In the presence of the small perturbation H, the convergence rate towards the fixed point of (4) would be given by $\tau_0^{-1}(2r + 3H/A_\infty)$ which would give the three supplementary estimates quoted in the fourth line of the table above. While the first one (closest to critical) is positive and has a satisfactory order of magnitude, the two next are negative and strongly depart from one's expectation as ε is increased. Basically, the measured final rates $1/\tau_{\rm end}$ are much too small. It will be shown in the next section that this is due to phase relaxation that actually controls that stage of the evolution and not amplitude relaxation as assumed by the Landau picture.

The essential part of the discrepancy between onset and decay rates reported in [1] therefore stems from the fact that most of the decay corresponds to on-the-spot collapse of the solution without much morphological change so that the Landau approach is valid as a first approximation. In particular, critical slowing-down is indeed observed for most of the decay transient except near the end and for R_f very close to R_c or below threshold ($R = 67.9, 68.1, 68.3$) where perturbations linked to induction by end vortices have sizeable effects. In contrast, at moderate aspect ratio, this perturbation can never be neglected at onset: the initial growth rate of the solution depends on it and remains finite for $R \sim R_c$. Furthermore, fitting the evolution of V_m against the solution to (2) implies *systematic errors* rendering the time-constant estimate incorrect, especially as time increases and the stationary state is approached. Since the induction by end vortices is increasingly important as Γ is decreased, one should not be surprised that an effect already visible at $\Gamma = 24$ should be detected for the values considered by Abshagen et al. that were all smaller.

5 Aspect-ratio dependence at onset

We now consider a series of onset experiments starting from equilibrium solutions at $R_i = 67.2$ with $R_f = 68.7$ and various aspect ratios ranging from 8 to 40. Figure 5 again clearly shows that the expected linear behaviour of $\frac{\rm d}{{\rm d}t} \ln V_m$ inherent in (3) is never verified. The "less worst" case is for $\Gamma = 8$, which can be understood from the fact the solution does not change its shape drastically so that the evolution can be characterised by a single amplitude solely function of time. This can be expected from the strong lateral boundary effects known to be dominant at small aspect ratio. Obviously, the Landau test becomes worse as the aspect ratio increases, so that a single time scale based on the measurement of V_m cannot be used to characterise the onset transient. The aim of this section is to identify its different stages and associated times. We start with the examination of the worst case available, $\Gamma = 40$, then gather results for the other values of the aspect ratio, and finally interpret the behaviour of the onset times which shows up in the late relaxation stage $t \to \infty$, when Δ_m approaches

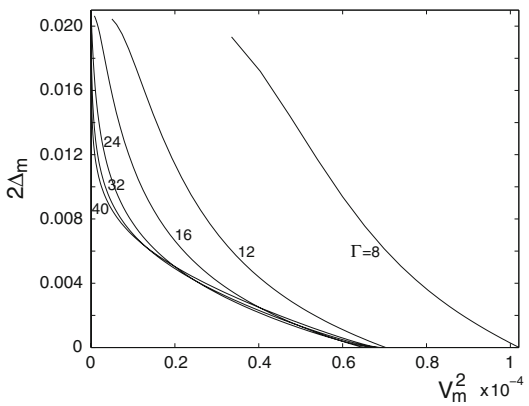

Fig. 5 Test of the Landau theory, i.e. plot of $V_m^{-2}\frac{\rm d}{{\rm d}t}V_m^2 = 2\Delta_m$ as a function of V_m^2, for onset from the equilibrium solution at $R_i = 67.2$ taken as initial condition, to the final steady state at $R_f = 68.7$, $\Delta_m \approx 0$, for the series of Γ under study

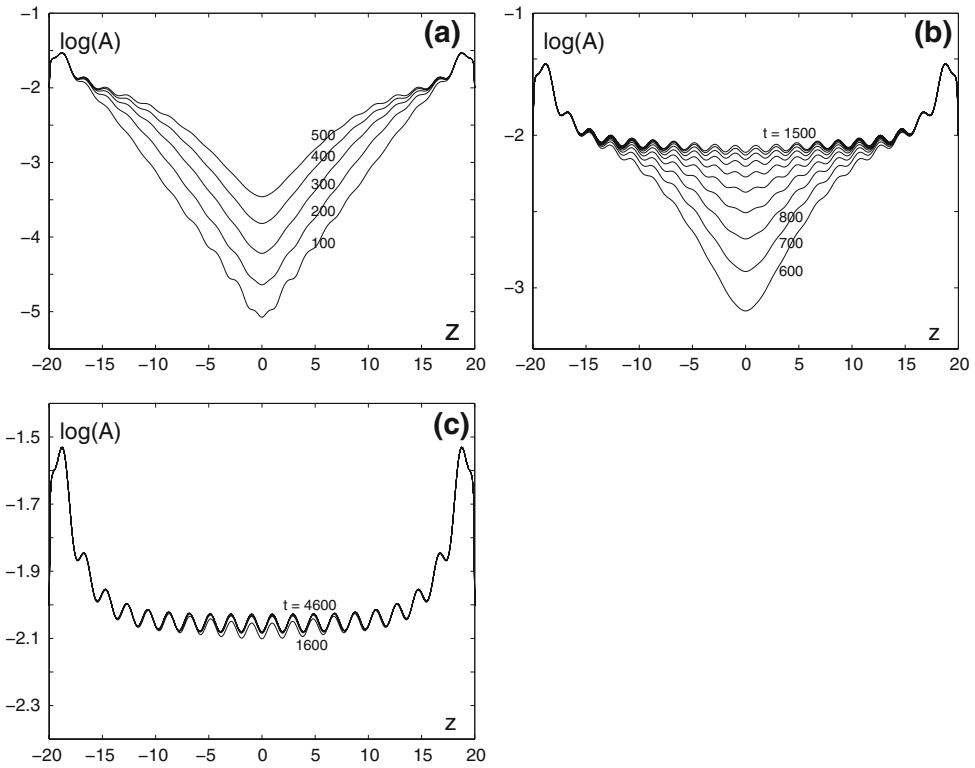

Fig. 6 Onset from $R_i = 67.2$ to $R_f = 68.7$ for $\Gamma = 40$ starting from the equilibrium solution at $R = R_i$. **a** Snapshots of the amplitude of the solution for t from 100 to 500 with $\Delta t = 100$, showing the propagating front from the ends towards the centre. **b** For $t = 600$ to 1,500, with $\Delta t = 100$, the amplitude of the solution gets essentially uniform. **c** For $t = 1{,}600$ to 4,600 with $\Delta t = 500$, the solution continues to evolve but now at roughly constant amplitude, all curves are stacked on each other except for $t = 1{,}600$. The remaining trace of modulations in $|A(z, t)|$ comes from incomplete demodulation as explained in Sect. 3

zero while V_m^2 tends to a value around 6.5×10^{-5}, only slightly dependent on Γ as anticipated in the limit of a laterally unbounded TC set-up. (This value is reasonable agreement with the equilibrium value derived from the Landau fit for decay $A_0\sqrt{\varepsilon} \approx 6.3 \times 10^{-5}$ with $g = 1/A_0^2 \approx 120$ for $R = 68.7$ and the theoretical threshold value at infinite aspect ratio $R_c^\infty = 68.186$).

It has been known for long [20] and can also be seen in Fig. 4 presented in [1], that the onset transient may be understood as resulting first from the propagation of the bifurcated solution induced by Ekman pumping at the end disks towards the interior where, when the cylinders are long enough, the flow is still essentially in the base state (pure azimuthal Couette flow). This phenomenon is illustrated for $\Gamma = 40$ in Fig. 6a where the plot of the logarithm[7] of $|A(z, t)|$ clearly suggests two exponential tails translating one towards the other at constant speed. Careful analysis however shows that this is only a rough guess since the shape and speed of the amplitude's front both slightly change during the early part of the transient. This is in line with an observation by Niklas et al. [21] who studied front propagation in semi-infinite geometry and indeed showed that setting the front into motion takes a while. Identification of the regime of steady state propagation in our large-but-not-so-large systems will however be attempted later (in Fig. 9). After the fronts have met in the middle, the amplitude gets nearly uniform as seen in panel (b). The last evolution stage displayed in panel (c) corresponds to a slow convergence of the solution towards its final shape.

On the other hand, though we have shown this to be incorrect, the evolution of $V_m(t)$ displayed in Fig. 7a resembles what could be expected for a Landau amplitude governed by (2): it first grows exponentially in time, then goes through an inflection point, here at $t \approx 978$ (mark '$*$'), and finally saturates. The initial exponential growth is fully apparent as a linear increase of $\ln[\frac{\mathrm{d}}{\mathrm{d}t} V_m]$ with slope 1.02×10^{-2} (Fig. 7b). This value cannot be compared directly to $\varepsilon/\tau_0 \approx 3 \times 10^{-3}$ as expected from the plain Landau theory since the growth of the amplitude at the middle corresponds to the approach of the two exponential tails of the fronts coming from the ends.

[7] Here and at a few other places we use the decimal logarithm 'log' instead of the natural logarithm 'ln' since it allows a more familiar estimation of orders of magnitude.

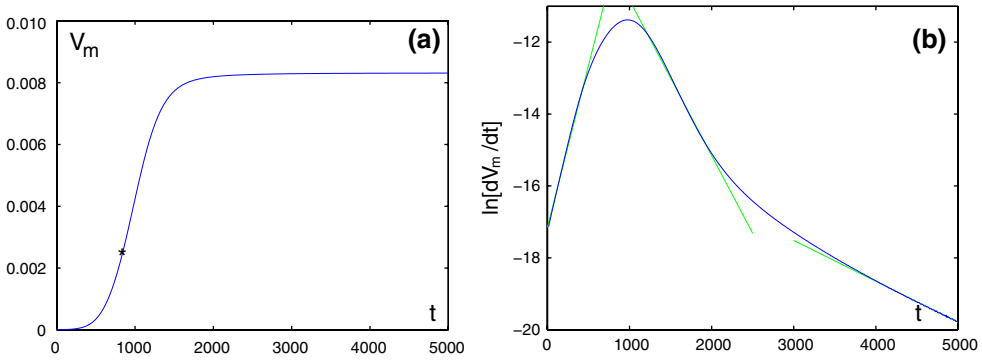

Fig. 7 **a** V_m as a function of time at onset from $R_i = 67.2$ to $R_f = 68.7$ for $\Gamma = 40$. **b** corresponding time series of $\ln[\frac{\mathrm{d}}{\mathrm{d}t} V_m]$, the three local slopes indicated by lines are 1.02×10^{-2} for $t \to 0$, -4.3×10^{-3} for $t \sim 1{,}500$ and -1.05×10^{-3} for $t \sim 4{,}500$

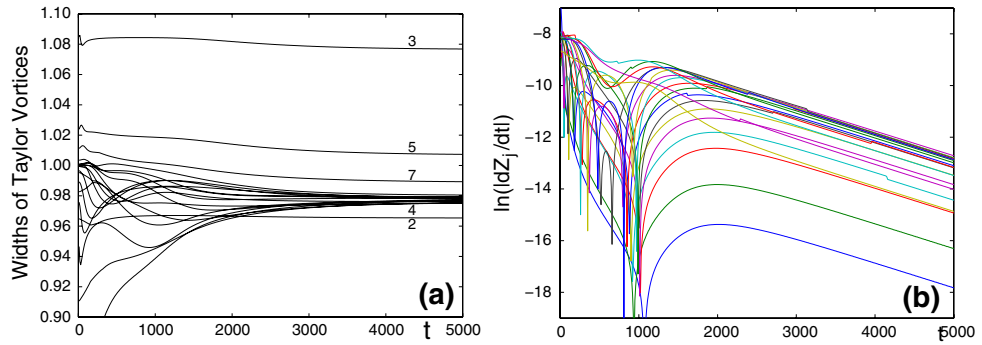

Fig. 8 **a** Widths of Taylor Vortices as functions of time during onset ($\Gamma = 40$). **b** Ultimate relaxation of the solution's zeros as seen from the variation $\ln[|\frac{\mathrm{d}}{\mathrm{d}t} z_j|]$ with time (only twenty curves for the forty zeroes appear owing to the "$z \mapsto -z$" symmetry that is perfectly fulfilled all along the simulation; the cusp observed for some curves corresponds to the fact that $\frac{\mathrm{d}}{\mathrm{d}t} z_j$ may change sign in the course of its evolution so that the log of its absolute value displays a singularity when the derivative goes through zero

Assuming that these tails are of the form $\exp[-(z - vt)/\xi]$ with $v \approx 2\xi_0\sqrt{\varepsilon}/\tau_0$ [21] and $\xi = \xi_0/\sqrt{\varepsilon}$ as derived from (6), one gets an effective growth rate at the given position, here the centre, $1/\tau_{\mathrm{eff}} = 2\varepsilon/\tau_0 \approx 6 \times 10^{-3}$, closer to the measured value but still somewhat smaller. The discrepancy should be attributed to finite size effects which, in the absence of detailed analytical solution, cannot be evaluated. (Graham and Domaradzki [27] considered only the steady state solutions.) It turns out that V_m approaches its asymptotic value in a two-stage process clearly visible in Fig. 7b, first for $t \in [1200, 1800]$ at a rate $\approx -4.3 \times 10^{-3}$—a value that could be compared to $-2\varepsilon/\tau_0$ expected from the convergence rate toward the non-trivial Landau fixed point—and finally much slower for $t > 3{,}000$ at a rate $\approx -1.05 \times 10^{-3}$. Evidence of this ultimate evolution is best illustrated by the drift of the solution's zeroes and the corresponding wavelength adjustment.

This phase relaxation stage driving the evolution of V_m is pictured in Fig. 8. The variation of the vortex widths with time is displayed in panel (a), except for the terminal vortex which has practically constant width (1.299) and is not reported there. The figure gives the widths of the vortices labelled by their number counted from the end as in Fig. 3. Coming from the end to the middle, the roll widths rapidly concentrate around a single value: 0.9773 ± 0.0016 (average over the 26 central rolls), hence an equilibrium wavelength $\lambda \simeq 1.955$ at $R_f = 68.7$, slightly smaller than the critical value $\lambda_c = 1.9867$ for $\eta = 0.5$ [14] due to non-linear interactions above threshold at finite aspect ratio. Figure 8b displays the local evolution rate of the zeroes of $V(z, t)$ and it is clearly seen that the late relaxation towards their final position is exponential. Careful inspection of the corresponding rates, obtained as explained in Sect. 3, shows that two of them (z_4 and z_{17}) enter the final stage quite late, in fact as late as V_m and with a decay time $\tau_{z_j} \approx 993$ ($j = 4, 17$), intermediate between that of V_m, $\tau_v = 950 = (1.05 \times 10^{-3})^{-1}$, and the decay time of others zeroes that all evolve at the same rate: $\langle \tau_z \rangle = 1038.2 \pm 2.3$. In other words, the detailed evolution of the solution is certainly quite complicated and, at the large aspect ratio considered, the very ultimate relaxation stage is likely not yet reached but the overall process seems well understood as global phase dynamics. This will be confirmed by the trends governing the decay time as a function of Γ to be examined just after its role on the early onset stage.

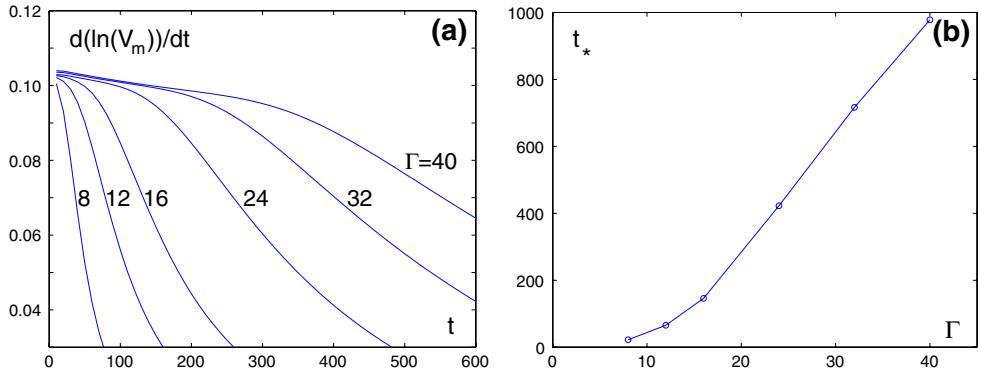

Fig. 9 **a** Growth rate of V_m for different values of Γ. **b** Variation with Γ of the duration of the initial front propagation stage as determined from the time t_* when V_m goes through the inflection point

The front propagation stage typical of the early transient can be identified for all the values of Γ considered except the smallest ones $\Gamma = 8$ and 12. On theoretical grounds, the speed depends on the relative distance ε to the ideal bifurcation point as $\varepsilon^{1/2}$ so that, at a given ε, the duration of the propagation stage is expected to scale as $\Gamma/\varepsilon^{1/2}$ though, as observed by Niklas et al. [21], setting the front into motion is not an immediate process. In our case of long but finite (and in practice not so long) systems, Fig. 9a supports the idea that the initial growth rate of V_m is controlled by front propagation as explained earlier and, as such, quite insensitive to Γ for $\Gamma \geq 16$: the longer the system, the longer the initial plateau (growth time $\tau \approx 98$). If we make the supplementary assumption that this early stage ends when V_m goes through the inflection point (marked with an asterisk in Fig. 7a for $\Gamma = 40$), denoting t_* the corresponding time, we get:

Γ	8	12	16	24	32	40
t_*	22.4	65.5	146.0	422.6	716.4	977.8

The expected linear behaviour is indeed present for $\Gamma \geq 16$ as shown in Fig. 9b. While it is somehow arbitrary to define the end of the front propagation stage through t_*, the observed scaling behaviour should be robust against a change of definition.

Let us now consider the final relaxation rates that are also well defined quantities. The table below gathers our results obtained by measuring both V_m and the drift of the zeroes (excluding a few "outliers", see the discussion for $\Gamma = 40$), respectively called τ_v and $\langle \tau_z \rangle$:

Γ	8	12	16	24	32	40
τ_v	75	146	215	380	652	951
$\langle \tau_z \rangle$	74	145	216	377	650	1038

The general agreement between the two estimates undoubtedly shows that the final relaxation stage is a global process. (The case $\Gamma = 40$ with τ_v substantially smaller than $\langle \tau_z \rangle$ has already been discussed and the discrepancy attributed to insufficient convergence of the late stage).

Theoretical considerations initiated in [30] suggest that wavelength relaxation is governed by a diffusive process:

$$\partial_t \phi = D_\parallel(q_0, \varepsilon)\partial_{zz}\phi \,, \tag{8}$$

where ϕ is the *phase* of the solution with essentially the same meaning as in (6) where A was defined as the complex envelope of the solution, and where $D_\parallel$ is the diffusion coefficient for compression/expansion perturbations. If this is the case, it seems legitimate to admit that the phase is clamped at the end-disks and that the slowest diffusion mode is a simple cosine arch with wavelength $\sim 2\Gamma$, so that the relaxation rate is $\tau^{-1} = D_\parallel(\pi/\Gamma)^2$, hence $\tau/\Gamma^2 \sim$ Cst. This guess is checked in Fig. 10 which displays $\langle \tau_z \rangle/\Gamma^2$ as a function of Γ, clearly showing that for $\Gamma \geq 24$ the theoretical expectation is fulfilled.

In practice, whereas the trend is clear, sustaining the claim at a quantitative level turns out to be a hard task for several reasons. First, empirically the plateau observed at large Γ still display irregularities that, though

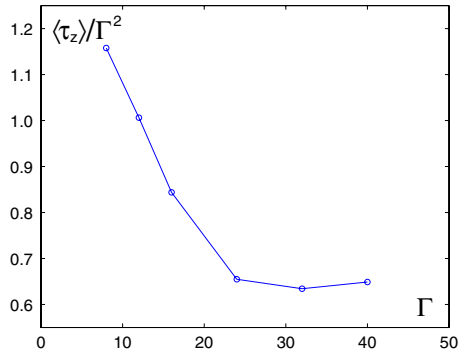

Fig. 10 Empirical evidence from the variation of $\langle\tau_z\rangle$ with Γ that the late relaxation stage is essentially a diffusive process

being only a few percents of the "asymptotic" value of $\langle\tau_z\rangle/\Gamma^2$, cannot be attributed to measurement errors[8] and the limited range of Γ that we have considered may not be large enough. It might further be that, while keeping the analytical expression of the estimate, Γ had to be replaced by some effective value $\Gamma_{\rm eff} < \Gamma$ taking a better account of the specific nature of the forcing and modifying the simple boundary condition imposed to the phase. (This is in contrast with what will be obtained in the next section for decaying solutions when $R_f < R_c$ where the final diffusion process will prove well fitted against a linearized Ginzburg–Landau equation allowing us to define an effective aspect ratio, which will be legitimate for final states below the threshold where non-linearities will be weak everywhere except in the two end vortices.) The observed irregularities will find another illustration in Sect. 7 when non-integer aspect ratios will be considered. In fact the main difficulty, of theoretical origin, is that—to our knowledge—the phase diffusion formalism has not been quantitatively implemented in the TC case since it requires a lot more (but not much rewarding) computations than for variants of the Swift–Hohenberg model such as the one considered by Rucklidge and Champneys [18] and for which computations are at their simplest [30]. As a matter of fact, though for dimensional reasons $D_\parallel$ scales as ξ_0^2/τ_0, where ξ_0 and τ_0 are the two main parameters in the Ginzburg–Landau equation (6), the actual value is still dependent on the precise value of the wavelength of the underlying periodic pattern. It turns out that this value is sensitively dependent on Γ: in the middle of the cell we get $\lambda = 1.918$, 1.938, and 1.995 for $\Gamma = 24$, 32, and 40. The actual value of the diffusion coefficient would thus have also to be determined with this wavelength dependence in mind, which would imply a double expansion in powers of the distance to threshold *and* critical wave-vector as done for RB convection [37], but goes much beyond what is necessary for the envelope equation at lowest non-trivial order, see [23] and also [38] for an incomplete attempt specific to the TC problem.

6 Decay for $R_f < R_c$

Decay toward sub-critical values of R_f was examined by Abshagen et al. [1] only on the basis of numerical simulations of the Navier–Stokes equations using the model proposed by Schaeffer [15] in circumstances approaching the realistic no-slip conditions. They limited themselves to the illustration of how evolutions of spatial patterns differ at onset and decay for $\Gamma = 16$. Here we consider this problem in more detail, again characterising the overall deformation of the solution using both V_m and the widths of the Taylor cells.

We begin with the equivalent of Fig. 5 for the decay from $R_i = 68.7$ to $R_f = 67.2$, displayed in Fig. 11. Panel (a) displays the full range of variation of Δ_m as a function of V_m^2 for the whole set of values of Γ while Panel (b) zooms on the part $V_m^2 < 4.\,10^{-4}$ for the three largest values of Γ. The Landau test—whether the variation is linear or not—is not so bad for $\Gamma = 8$, very bad for $\Gamma = 12$ and 16, whereas it improves for $\Gamma = 24$ and becomes apparently good for the largest values $\Gamma = 32$ and 40 except when V_m^2 approaches zero (late decay stage).

The test is not so bad for $\Gamma = 8$ because the boundaries are so close that the shape of the solution (not shown here) does not change much during the decay, which is indeed a necessary condition for naive Landau theory to hold. The same reason explains why the value asymptotically reached by V_m is still sizeable. Understanding

[8] Error bars mentioned previously when defining $\langle\tau_z\rangle$ and discussing the case $\Gamma = 40$ cannot be made visible at the scale of the figure.

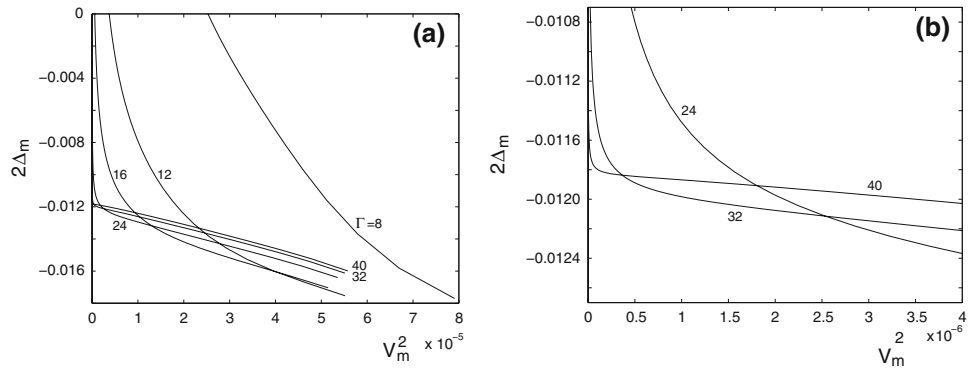

Fig. 11 Test of Landau theory (3) for decay from $R_i = 68.7$ to $R_f = 67.2$. **a** Full range evolution for the series of Γ under study. **b** Zoom on the late decay stage for the largest Γs

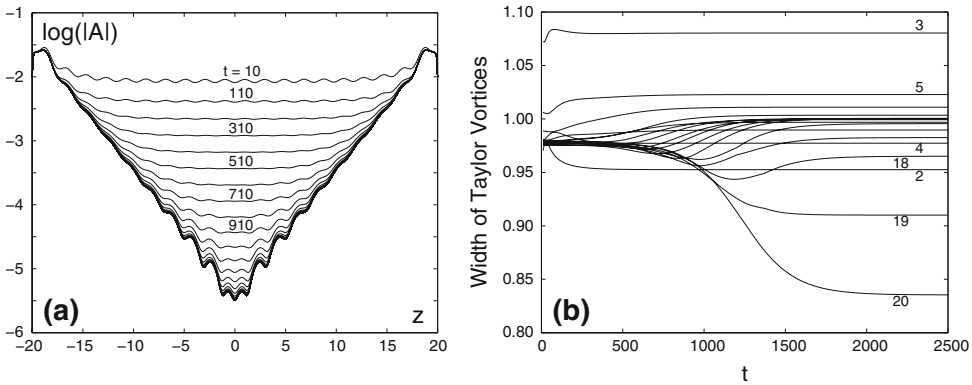

Fig. 12 **a** Amplitude of the solution at different times during decay from $R_i = 68.7$ to $R_f = 67.2$ for $\Gamma = 40$. **b** Widths of Taylor vortices as a function of time during decay; numbers label vortices from the end; the width of the end vortex, always much larger, is not shown

why it is bad for the intermediate values $\Gamma = 12$ and 16 and seems to improve for $\Gamma = 24$, 32, and 40, follows from our previous study of the case $\Gamma = 24$. Let us consider Fig. 12 for $\Gamma = 40$. Figure 12a displays the modulus of the envelope of $V(z, t)$ extracted by Hilbert transform at a series of equally spaced times, and clearly illustrates the (approximately) exponential on-the-spot relaxation of the central part till around $t = 1{,}000$. Panel (b) shows that the widths of Taylor vortices, at first clustering around the value reached at the end of the onset experiment (Fig. 8), begin to move only in a second stage. Accordingly, during early decay V_m is a genuine proxy to the amplitude of the solution in the central part. In that region, the solution remains close to an ideally periodic uniform pattern *with constant wavelength*, even if this wavelength is slightly shifted from its value at threshold. The behaviour predicted by the Stuart–Landau Eq. (2) is thus expected to hold since the shape of the envelope stays uniform. This stage is further essentially independent of the length of the system for Γ large enough: the curves for $\Gamma = 24$, 32 and 40 stay close to each another, being essentially linear with identical slopes for $V_m^2 > 5 \times 10^{-6}$, see Fig. 11a. From (3), these slopes corresponds to the non-linear coefficient g in (2), expected to be independent of Γ. On the other hand, again from (3), the slight shift between the curves for $\Gamma \geq 24$ is easily interpreted as due to a change of the effective distance to threshold implied by the wave-vector shift of the pattern in the initial state (*phase-winding solutions*), constant during early decay as already noticed, $\varepsilon_{\text{eff}} = \varepsilon - \xi_0^2(q_0 - q_c)^2$, q_0 staying close to q_c but sensitively dependent on Γ.

In contrast with early decay mostly related to the amplitude, late decay deals with the phase of the solution, i.e. the widths of Taylor vortices. Figure 12b display their variation as a function of time. The starting values are those shown at the large-t end of the graphs in Fig. 8a. The width of vortex 1, the closest to the end disks, is not represented since it adjusts practically immediately to 1.277, down from 1.299, which merely reflects the change in R. Vortices 2 to 5 also reach their final widths extremely fast, as the Ekman boundary layer forms immediately after the beginning of the experiment, exponentially decaying in space over few vortices. The other vortices are sub-critical Taylor rolls induced by the forcing. They reach their asymptotic widths

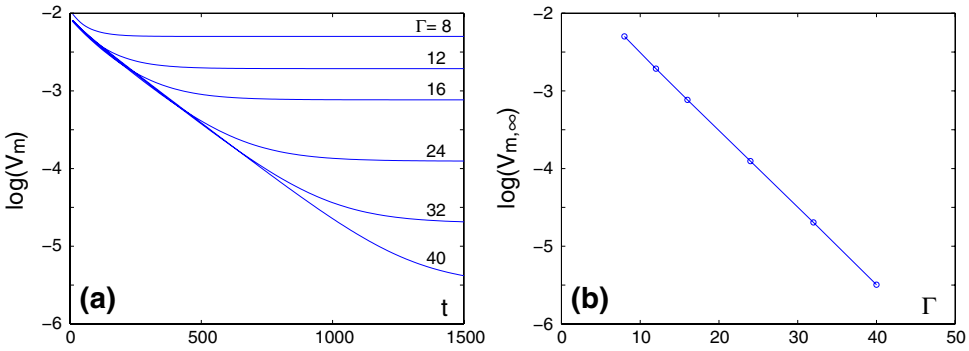

Fig. 13 **a** Evolution of V_m during the decay from $R_i = 68.7$ to $R_f = 67.2$ for all the values of Γ considered. **b** Values V_m^∞ of V_m reached in the limit $t \to \infty$ as a function of Γ for $R = R_f = 67.2$ (in practice $t = t_{\max} = 1{,}600$ for $\Gamma \leq 32$ and $t_{\max} = 3{,}000$ for $\Gamma = 40$)

more progressively, clustering around 1 (0.9997 ± 0.0023 for vortices 8 to 16, that compares favourably with the value 0.9934 predicted by Dominguez-Lerma et al. [14] for $\eta = r_i/r_o = 0.5$). Some compression is observed for the most central vortices that adjust their widths in the late relaxation stage: In fact, the system has to deal with a mismatch between the imposed aspect ratio Γ and an integer number of vortices at the critical wavelength favoured by the instability mechanism close to threshold. This mismatch is linked to the anomalously large width of the end vortices. Section 7 will provide us with a more dramatic illustration of it.

The zoom on the region $V_m^2 < 4 \times 10^{-6}$ in Fig. 11b corresponding to the late stage of the decay suggests a study of final relaxation rates that parallels the one performed for onset. Figure 13a displays the semi-log plot of V_m as a function of time and illustrates the decay towards an equilibrium value that decreases exponentially with Γ. This feature, clearly seen in Fig. 13b and easily guessed from Fig. 7 in [18], can be understood from an approximate steady state solution to the Ginzburg–Landau Eq. (6) with lateral forcing below threshold. Apart from boundary layers of essentially constant width close to the end disks, where non-linear terms are not negligible, the equation governing the steady-state solution ($\partial_t A \equiv 0$) can be reduced to $\varepsilon A + \xi_0^2 \partial_{zz} A = 0$ with $\varepsilon < 0$ and the actual solution close to the end-disks replaced by an effective boundary condition $A = A_{\rm eff}$ independent of R at a fixed distance from them. The evaluation at mid-length $\Gamma/2$ of the approximate solution in terms of hyperbolic cosine then yields the observed exponential behaviour with Γ. A more precise study taking into account non-linearities in the end region, copying that in [27] or [28], would possibly explain deviations at very small values of Γ but more sophistication does not seem necessary here since the expected exponential behaviour already holds for $\Gamma = 8$.

Let us now study the decay rate of V_m towards its asymptotic value as a function of Γ. As explained at the end of Sect. 3, the troublesome effects of constants such as V_m^∞ on the evaluation of the decay rates are discarded by considering $\frac{\rm d}{{\rm d}t} V_m$ instead of V_m. The analysis strictly parallels that developed for onset and we just give the result in the form of a table displaying decay times τ_v for V_m and $\langle \tau_z \rangle$ for the position of the zeroes of $V(z,t)$.

Γ	8	12	16	24	32	40
τ_v	63.5	104.9	131.3	154.5	162.5	166.9
$\langle \tau_z \rangle$	63.4 ± 0.1	104.3 ± 0.4	128.6–133.1	150.8–156.9	155.7–169.1	161.0–177.2

The behaviour of the final relaxation time τ_v can be derived from the time-dependent adaptation of the argument predicting the exponential behaviour of V_m^∞ as a function of Γ. Indeed, let us assume that, in the late stage, the distance to the equilibrium state $\delta A(z,t) = A(z,t) - A(z,\infty)$ evolves according to the linearized equation:

$$\tau_0 \partial_t \delta A = \varepsilon \delta A + \xi_0^2 \partial_{zz} \delta A ,$$

and that the effective boundary conditions on $\delta A(z,t)$ is $\delta A(z = \pm z_{b,\rm eff}, t) = 0$ with $z_{b,\rm eff} = \frac{1}{2}(\Gamma - \delta\Gamma)$, where $\delta\Gamma$ is a correction intended to account for the forcing by the Ekman end vortices. Then δA is easily seen to be of the form:

$$\delta A(z,t) = \delta A_0 \cos\left[\tfrac{1}{2}\pi z / z_{b,\rm eff})\right] \exp(\sigma t) ,$$

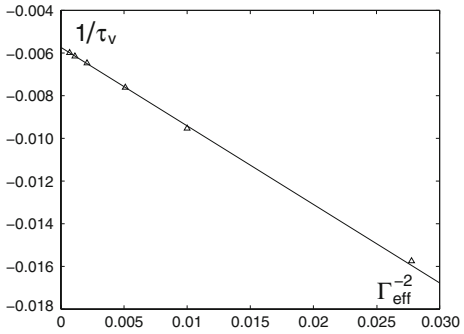

Fig. 14 Asymptotic value of τ_v as a function of $\Gamma_{\rm eff}^{-2}$, with $\Gamma_{\rm eff} = \Gamma - \delta\Gamma$ and $\delta\Gamma = 1.95$

with the corresponding estimation of the relaxation rate σ:

$$\tau_0\sigma = \varepsilon - \xi_0^2 \left(\pi/2z_{b,\rm eff}\right)^2 .$$

Figure 14b shows that the fit of σ against $a - b/(\Gamma - \delta\Gamma)^2$ with $a = -0.005735$, $b = 0.3716$, and $\delta\Gamma = 1.95$ is extremely satisfactory, which supports the estimate and the heuristic approach behind it: Based on our previous results we would predict $a = \varepsilon/\tau_0 \approx 5.6 \times 10^{-3}$ and using $\xi_0 = 0.377$ given in [14] we would get $b = \xi_0^2\pi^2/\tau_0 \approx 0.54$ which has the right order of magnitude and is not too bad a prediction owing to the crudeness of the assumptions made. Another check is obtained from the asymptotic limit $\Gamma \to \infty$ which yields $\tau_v^\infty = 1/|a| \approx 174.4$, in good agreement with the value $\tau_0/\varepsilon = 186.5$ obtained from our evaluation of τ_0 at $\Gamma = 24$ for $R = R_f = 67.2$.

The relaxation times of the velocity at mid-gap and mid-length and of the drift of the zeroes given in the table above are again the same order of magnitude. At the largest aspect ratios some dispersion of the $\tau_{z,j}$ is observed but always in a narrow range that nicely brackets the corresponding value of τ_v.

Though the actual dependence of the solution on z and t is certainly complicated, as already inferred from the separate evolution of the modulus of the envelope and the widths of vortices presented in Fig. 12 for the most extreme case at our disposal, $\Gamma = 40$, it has been shown that the Ginzburg–Landau formulation already gives a consistent set of information for $\varepsilon < 0$.

7 Non-integer aspect ratios

Up to now we have considered values of the aspect ratio Γ approximately fitting an integer number of vortices (approximately since the end vortices were seen to be a little wider, hence the correction $\delta\Gamma$ introduced in the analysis of decay experiments). Here we consider the complementary interesting case of onset experiments from $R_f = 67.2$ for Γ_k varying between 24.4 and 25.6, every $\Delta\Gamma = 0.4$, which combines the effects of non-linearity and non-integer aspect ratio. This problem was already studied by Zaleski [29] in an abstract setting within the framework of the complex envelope formalism using artificial complex $\mathcal{O}(1)$ boundary conditions as a model. Here we examine the concrete case of Taylor vortices with realistic end boundaries. We worked by increasing the aspect ratio step-wise. Values $\Gamma_k = 24.4, 24.8, 25.2$ and 25.6 were studied in addition to $\Gamma = 24$ already considered in Sect. 4. Initial conditions were prepared by letting the solution evolve at $R = R_i = 67.2$, from a given aspect ratio Γ_k by impulsively setting Γ to the next value Γ_{k+1}, starting from $\Gamma_0 = 24$. The envelopes and vortex widths of the corresponding initial conditions are displayed in Fig. 15. The largest part of the envelope corresponds to an exponential decrease corresponding to a response to the induction by end vortices, Fig. 15a. Notice however the behaviour of the curves for $\Gamma = 24$ and $\Gamma = 25.6$ which show seemingly anomalous dips near the centre. These dips can be understood from the relation between the modulus and phase of the complex envelope, itself related to the local wavelength of the vortices in the steady-state solution, Fig. 15b: the end vortices have essentially constant widths and all vortices have wavelength clustering around $\lambda_c/2 \approx 1$ except those at the centre which strongly and regularly depend on the value of the aspect ratio. The solutions thus adjust themselves at their weakest point where $|A|$ is minimum, in order to 'please' the instability mechanism that requires $\lambda \simeq \lambda_c$ in the largest possible region, while taking into account end effects that generate slightly wider vortices. The most extreme dip is obtained for $\Gamma = 25.6$ which, being close to 26 would favour thirteen pairs of vortices and thus accommodate twelve pairs of strongly stretched rolls.

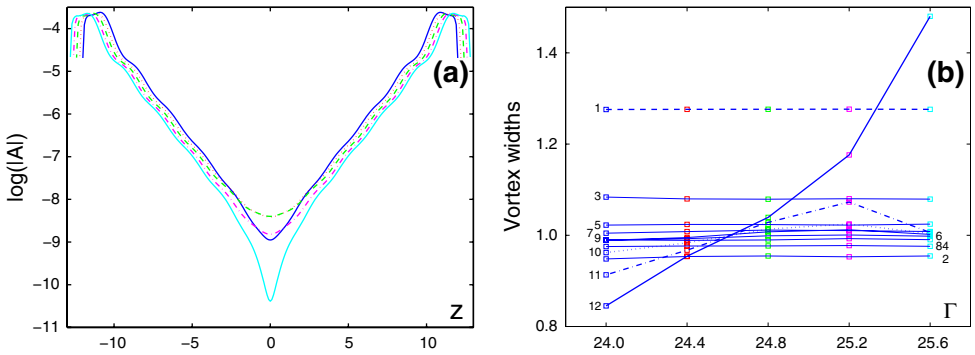

Fig. 15 **a** Amplitude of the initial conditions at $R = R_i = 67.2$ [$\varepsilon = -1.45 \times 10^{-2}$] for the different values of Γ from $\Gamma = 24$ (*solid, blue*) to 24.4 (red, hidden, except close to the ends), 24.8 (*green, dashed*), 25.2 (magenta, dash-dotted) and 25.6 (*solid, cyan*). **b** Corresponding vortex widths (half of them, labeled from 1 (*end*) to 12 (*centre*)

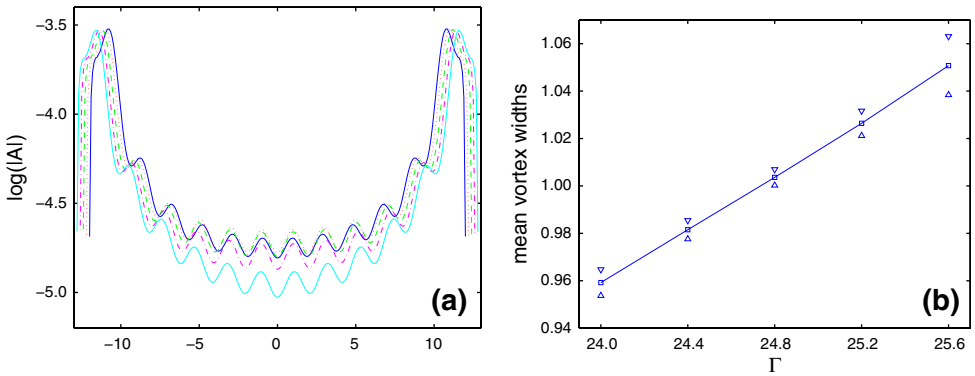

Fig. 16 **a** Amplitudes at steady state for onset to $R_f = 68.7$ [$\varepsilon = 7.54 \times 10^{-3}$]. **b** Vortex widths $\lambda_m/2 = \pi/q_m$ at steady state as functions of the aspect ratio

Indeed, from a variational point of view valid for a complex Ginzburg–Landau equation with real coefficients, it would be more costly to distribute the extension/compression over the whole system rather than to localise it at the centre [23]. Let us now turn to onset experiments. In a first series we have considered the whole set of Γ values with $R_f = 68.7$ ($\varepsilon = 8 \times 10^{-3}$). A second experiment concerned the case $\Gamma = 25.6$, $R_f = 67.3$ ($\varepsilon = 2.2 \times 10^{-3}$) in an attempt to be closer to the region where Zaleski's asymptotic theory [29] based on the envelope formalism is expected to be valid.

• The steady state amplitude solutions of onset experiments for $R_f = 68.7$ and the series of Γ values are displayed in Fig. 16, panel (a) and the corresponding vortex widths in its panel (b). The latter were obtained as the average of the values over the twelve centre vortices, with quite small relative dispersion, showing a well defined trend from compressed for $\Gamma = 24$ ($\lambda_m/\lambda_c = 0.96$) to expanded for $\Gamma = 25.6$ (1.056), as a result of the adjustment to boundary conditions in combination with non-linear effects (see also Fig. 18b). Time scales for the convergence toward the steady state are given in the table below:

Γ	24.0	24.4	24.8	25.2	25.6
$\langle\tau_z\rangle$	377 ± 3	335 ± 2	337 ± 2	378 ± 3	549 ± 1

estimations based on the convergence of V_m giving the same quantitative results. Theoretical data required to make detailed comparisons sufficiently far beyond threshold (in the infinite aspect-ratio limit) are not available and we are restricted to qualitative checks. Figure 17a displays V_m measured at the end of the onset experiment (open circles) as a function of the distance to the critical wave-vector computed from the mean vortex width $\lambda_m/2 = \pi/q_m$ in Fig. 16b, compared to the prediction from the relation $A = A_0\sqrt{\varepsilon - \xi_0^2(q_m - q_c)^2}$, computed with A_0 as obtained earlier and the theoretical values of $R_c = 68.186$ and $\xi_0 = 0.377$ given by [14] (line and asterisks).

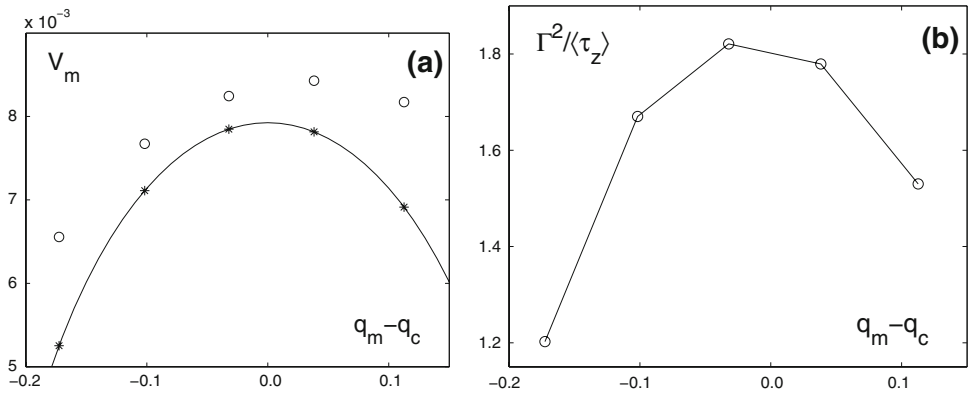

Fig. 17 **a** Comparison of measured (open circles) and predicted amplitudes (line and asterisks) at the centre at steady-state as functions of the measured distance to critical wave-vector. **b** Corresponding inverse relaxation times re-scaled by Γ^2 (dimensionally an effective phase diffusion coefficient) at onset to $R_f = 68.7$ for the series of aspect ratios Γ_k under consideration

Figure 17b displays $\Gamma^2/\langle\tau_z\rangle$ as a function of $q_m - q_c$. While quantities of the order of unity are obtained, a strong dependence on the actual value of the average wave-vector, itself a function of the aspect ratio, is observed. This dependence is compatible with what is known from the theory of the Eckhaus instability which is the trace of the diffusion coefficient $D_\parallel$ becoming negative. Close to threshold, the universal expression of $D_\parallel(\varepsilon, q)$ reads [23]:

$$D_\parallel(\varepsilon, q) = \frac{\xi_0^2}{\tau_0}\,\frac{\varepsilon - 3\xi_0^2(q-q_c)^2}{\varepsilon - \xi_0^2(q-q_c)^2}\,.$$

The variation of the numerator of this expression with $q_m - q_c$ at given ε mostly explains the observed trend but the connection is not easy to make at a quantitative level. In particular, the strong decrease of $\Gamma^2/\langle\tau\rangle$ for $q_m - q_c \sim -0.2$ is compatible with the approach to the Eckhaus stability boundary but, when using the theoretical values of the parameters, the predicted $D_\parallel$ is negative so that the instability should already have taken place. Though the trends are correctly reproduced, observed discrepancies should then be attributed to the fact that the experiment was performed at too small a value of Γ and that corrections due to the induction processes at the ends—the imperfection pointed out in Sect. 4—cannot be neglected. It should also be considered that the dynamics of the system is most certainly quantitatively modified by the proximity of the saddle-node bifurcation where the solution gains a pair of vortices, so that the implicit assumption of weak non-linearity underlying the analysis may fail and higher order processes may need to be included. However we are not aware of studies related to this specific problem in the Couette–Taylor context.

- The steady state solution for $\Gamma = 25.6$ and $R = 68.3$ is displayed and compared to that for $R = 68.7$ in Fig. 18. Corresponding solutions are shown in the bottom panels. The dip in the amplitude associated to the wavelength variation predicted by Zaleski's theory is clearly visible for $R = 68.3$ but disappear for $R = 68.7$. At finite distance from threshold, the amplitude and the wavelength are more uniform and the phase dynamics is expected to drive the system, as discussed above. Closer to threshold ($\varepsilon \to 0$) the amplitude and phase of the envelope are strongly coupled but end effects propagate deeps inside the system ($\xi = \xi_0/\sqrt{\varepsilon}$), which puts restriction on our simulation at $\Gamma = 25.6$. Just to give an idea of the time scales, combination of the critical slowing down and the approach to the Eckhaus instability, we now get $\langle\tau_z\rangle = 2117 \pm 24$. (The final relaxation stage was entered for $t \sim 2{,}000$ and the simulation was stopped at $t = 8{,}000$). Furthermore, the beginning of the evolution of V_m (not represented here) is not a good proxy to the overall evolution because during the early transient the profile of the solution is complicated so that a new pair of roll attempts to grow, but without success. It does not seem reasonable to try to compute over larger systems, longer times, and closer to threshold in order to go beyond this qualitative appreciation of the theory.

8 Conclusion

The present paper has been devoted to the study of transients toward Taylor vortices along the branch of "normal" states. That branch derives continuously from the axisymmetric Couette flow through the standard

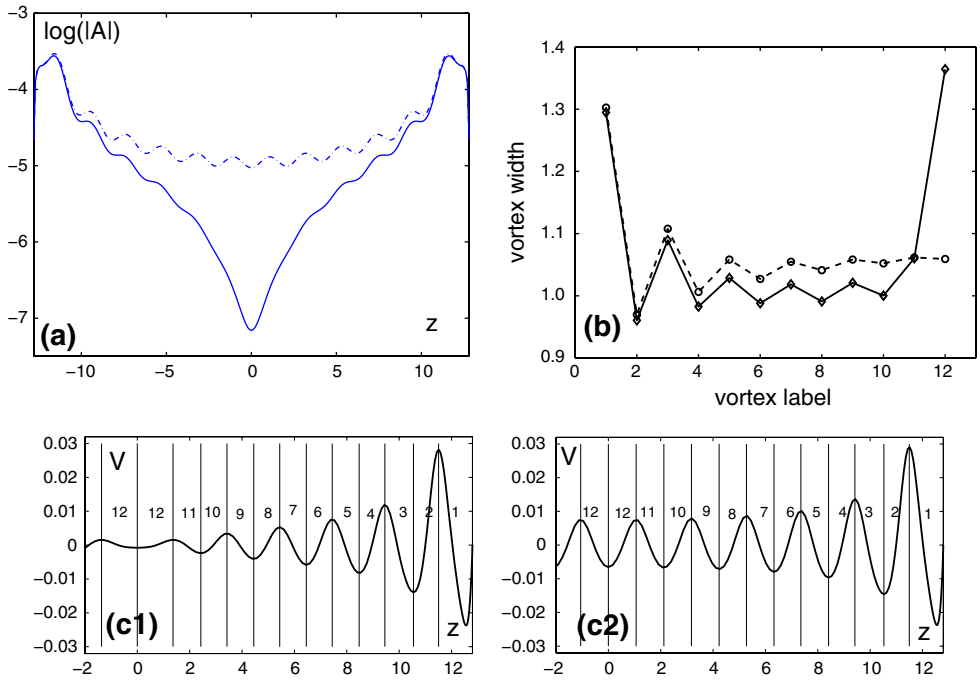

Fig. 18 Amplitudes **(a)** and vortex widths **(b)** at steady state for onset to $R_f = 68.3$ [$\varepsilon = 1.67 \times 10^{-3}$, *solid line*] and $R_f = 68.7$ [$\varepsilon = 7.54 \times 10^{-3}$, *dashed line*, already shown in Fig. 16a]. Corresponding solutions, $R = 68.3 \rightarrow$ (c1) and $R = 68.7 \rightarrow$ (c2)

super-critical bifurcation made imperfect by Ekman pumping at the end-disks. As it becomes clear from the consideration of Figs. 1, 7, and 11, the transition is not sharp and fitting the evolution of a single scalar quantity, e.g. the speed V_m at mid-gap and mid-length of the system, to the evolution expected from the Stuart–Landau normal form (2) accounting for a *perfect* super-critical bifurcation is inappropriate because the induction of vortices by a localised $\mathcal{O}(1)$ perturbation has non-trivial consequences. The simple *imperfect* unfolding of the perfect normal form (4) works as a first approximation for decay experiments because the spatial dependence and the temporal dependence remain uncoupled during early decay which forms the essentials of what is observed in experiments (Fig. 12). Difficulties with the plain Landau approach immediately arise when onset experiments are considered because the spatial dependence and temporal dependence cannot be separated during early transient marked by the propagation of the vortex strength from the end. In all cases, the late transient is a slow relaxation of the solution controlled by the aspect ratio Γ. When the final state is super-critical, a fine wavelength adjustment is involved through a *phase diffusion* process. In the sub-critical case, this is a mere relaxation towards the fundamental mode of the appropriate linearized Ginzburg–Landau equation. Consideration of non-integer aspect ratios pointed out supplementary peculiarities associated to the competition between solutions with neighbouring numbers of vortex pairs. In each circumstance, clearly identified limitations of the Landau approach appealed to its natural Ginzburg–Landau extension, relevant to analyse processes close to threshold in the large aspect-ratio limit.

While most of this study could have been performed in the mid-eighties, when pattern selection problems were topical, one should notice that, at that time, either steady states or permanently unsteady states (i.e. spatiotemporal chaos) were of most concern. Transients towards steady states, especially their dependence on the aspect ratio, were not under focus. The present study was thus triggered by the work of Abshagen et al. who did it for the Taylor–Couette problem. A good qualitative and semi-quantitative interpretation of their results has been obtained within the Stuart–Landau/Ginzburg–Landau framework [27,38]. Data analysis has been performed with care so that residual quantitative discrepancies can be attributed to the lack of theoretical data beyond lowest significant order. To our knowledge, in the Ginzburg–Landau formalism, the explicit expressions of the effective boundary conditions and of the additional non-linear bulk terms are not known, while these quantities are needed when Γ is finite, ε is finite, and the relevant times and/or distances are much larger than τ/ε and/or $\xi_0/\sqrt{\varepsilon}$. Except for models such as the Swift–Hohenberg model and some variants of it, e.g. the one used by Rucklidge and Champneys [18], the analysis has not been worked out sufficiently far—and in the latter case even only for the steady state—but developing it in the present context does not

seems much rewarding: our semi-quantitative checks based on purely phenomenological considerations prove already much valuable in explaining the behaviour of the time scales with the distance to threshold ε and the aspect ratio Γ.

Acknowledgments P. Manneville warmly thanks Tom Mullin and Jan Abshagen for interesting discussions about experimental results. A. Randriamampianina is deeply acknowledged for communicating information not published in [31] and related to regularisation. Computations were performed by O. Czarny within the framework of IDRIS contract #04242 *Study of laminar and transitional regimes in confined rotating flows* at M2P2, Marseilles. Part of his work was done during a post-doctoral stay at CEA-DRFC/SCCP (Association Euratom-CEA), Bat 513, CEA Cadarache 13108 St Paul Lez Durance Cedex, France.

References

1. Abshagen, J., Meincke, O., Pfister, G., Cliffe, K.A., Mullin, T.: Transient dynamics at the onset of Taylor vortices. J. Fluid Mech. **476**, 335–343 (2003)
2. Coles, D.: Transition in circular Couette flow. J. Fluid Mech. **21**, 385–425 (1965)
3. Andereck, C.D., Liu, S.S., Swinney, H.L.: Flow regimes in a circular Couette flow system with independently rotating cylinders. J. Fluid Mech. **164**, 155–183 (1986)
4. Prigent, A., Grégoire, G., Chaté, H., Dauchot, O., van Saarloos, W.: Large-scale finite-wavelength modulation within turbulent shear flows. Phys. Rev. Lett. **89**, 014501 (2002)
5. Chandrasekhar, S.: Hydrodynamic and Hydromagnetic Stability. Clarendon Press, Oxford (1961)
6. Drazin, P.G., Reid, W.H.: Hydrodynamic Stability. Cambridge University Press, Cambridge (1981)
7. Koschmieder, E.L.: Bénard Cells and Taylor Vortices. Cambridge University Press, Cambridge (1993)
8. Tagg, R.: The Taylor–Couette problem. Nonlinear Science Today **4**, 1–25; a reference list, fairly complete up to 1999, can be found at: http://carbon.cudenver.edu/~rtagg/tcrefs/taylorcouette.html (1994)
9. Stuart, J.T.: Nonlinear stability theory. Ann. Rev. Fluid Mech. **43**, 347–371 (1971)
10. Stuart, J.T.: On the non-linear mechanics of hydrodynamic stability. J. Fluid Mech. **4**, 1–21 (1958)
11. Kirchgässner, K.: Instabilität der Strömung swischen zweil rotierenden Zylindern gegenüber Taylor-Wirbeln für beliebige Spaltbreiten. ZAMP **12**, 14–30 (1961)
12. Davey, A.: The growth of Taylor vortices in flows between rotating cylinders. J. Fluid Mech. **14**, 336–368 (1962)
13. Donnelly, R.J., Schwarz, K.W.: Experiments on the stability of viscous flow between rotating cylinders. VI. Finite amplitude experiments. Proc. R. Soc. Lond. A **283**, 531–556 (1965)
14. Dominguez-Lerma, M.A., Ahlers, G., Cannell, D.S.: Marginal stability curve and linear growth rate for rotating Couette–Taylor flow and Rayleigh–Bénard convection. Phys. Fluids **27**, 856–860 (1984)
15. Schaeffer, D.G.: Qualitative analysis of a model for boundary effects in the Taylor problem. Math. Proc. Camb. Phil. Soc. **87**, 307–337 (1980)
16. Hall, P.: Centrifugal instabilities in finite containers: a periodic model. J. Fluid Mech. **99**, 575–596 (1980)
17. Benjamin, T.B., Mullin, T.: Anomalous modes in the Taylor experiment. Proc. R. Soc. Lond. A **377**, 221–249 (1981)
18. Rucklidge, A.M., Champneys, A.R.: Boundary effects and the onset of Taylor vortices. Phys. D **191**, 282–296 (2004)
19. Ahlers, G., Cannell, D.S.: Vortex front propagation in rotating Couette–Taylor flow. Phys. Rev. Lett. **50**, 1583–1586 (1983)
20. Neitzel, G.P.: Numerical computation of time dependent Taylor-vortex flow in finite-length geometries. J. Fluid Mech. **141**, 51–66 (1984)
21. Niklas, M., Lücke, M., Müller-Krumbhaar, H.: Velocity of a propagating Taylor-vortex front. Phys. Rev. A **40**, 493–496 (1989)
22. Hall, P.: Evolution equation for Taylor vortices in the small gap limit. Phys. Rev. A **29**, 2921–2923 (1984)
23. Manneville, P.: Dissipative structures and weak turbulence. Academic Press, Boston; see especially Chapters 4, 5, 8–10 (1990)
24. Daniels, P.G.: The effect of distant sidewalls on the transition to finite amplitude Bénard convection. Proc. R. Soc. Lond. A **358**, 173–197 (1977)
25. Hall, P., Walton, I.C.: The smooth transition to a convective regime in a two-dimensional box. Proc. R. Soc. Lond. A **358**, 199–221 (1977)
26. Cross, M.C., Daniels, P.G., Hohenberg, P.C., Siggia, E.D.: Phase winding solutions in a finite container above the convective threshold. J. Fluid Mech. **127**, 155–183 (1983)
27. Graham, R., Domaradzki, J.A.: Local amplitude equation of Taylor vortices and its boundary condition. Phys. Rev. A **26**, 1572–1579 (1982)
28. Pfister, G., Rehberg, I.: Space-dependent order parameter in circular Couette flow transitions. Phys. Lett. A **83**, 19–22 (1981)
29. Zaleski, S.: Cellular patterns with boundary forcing. J. Fluid Mech. **149**, 101–125 (1984)
30. Pomeau, Y., Manneville, P.: Stability and fluctuations of a spatially periodic convective flow. J. Phys. Lett. **40**, L609–L612 (1979)
31. Randriamampianina, E., Elena, L., Fontaine, J.P., Schiestel, R.: Numerical prediction of laminar, transitional and turbulent flows in shrouded rotor-stator systems. Phys. Fluids **9**, 1696–1713 (1997)
32. Tavener, S.J., Mullin, T., Cliffe, K.A.: Novel bifurcation phenomena in a rotating annulus. J. Fluid Mech. **229**, 483–497 (1991)
33. Czarny, O., Serre, E., Bontoux, P., Lueptow, R.M.: Interaction between Ekman pumping and the centrifugal instability in Taylor–Couette flow. Phys. Fluids **15**, 467–477 (2003)
34. Peyret, R.: Spectral methods for incompressible viscous flows. Series: Applied Mathematical Sciences, vol. 148. Springer, New York (2002)
35. Raspo, I., Hugues, S., Serre, E., Randriamampianina, A., Bontoux, P.: A spectral projection method for the simulation of complex three-dimensional rotating flows. Comp. Fluids **31**, 745–767 (2002)

36. Jackson, L.B.: Digital Filters and Signal Processing—with MatLab Exercises. Kluwer, Dordrecht (1996)
37. Manneville, P., Piquemal, J.M.: Zigzag instability and axisymmetric rolls in Rayleigh–Bénard convection, the effects of curvature. Phys. Rev. A **28**, 1774–1790 (1983)
38. Walgraef, D.: End effects and phase instabilities in a model for Taylor–Couette systems. Phys. Rev. A **34**, 3270–3278 (1986)